Article

The Effects of Tricalcium Silicate Nanoparticle-containing Cement: In Vitro and In Vivo Studies

Naho Ezawa [1,*], Yoshihiko Akashi [2], Kei Nakajima [2], Katsutoshi Kokubun [2], Masahiro Furusawa [1] and Kenichi Matsuzaka [2]

[1] Department of Endodontics, Tokyo Dental College, Japan
[2] Department of Pathology, Tokyo Dental College, Japan
* Correspondence: ezawanaho@tdc.ac.jp

Abstract: A tricalcium silicate nanoparticle-containing cement (NPC) was developed to overcome the disadvantages of existing mineral trioxide aggregate (MTA) dental materials. This study aimed at evaluating the effects of NPC on the osteogenic differentiation of human periodontal ligament fibroblasts (HPLFs) in vitro, and on the healing of furcal perforations created experimentally in rat molars in vivo, in comparison to MTA. The in vitro studies performed the following assays; pH measurement using a pH meter, the release of calcium ions using a calcium assay kit, cell attachment and morphology using SEM, cell proliferation using a coulter counter, marker expression using quantitative reverse transcription polymerase chain reaction (qRT-PCR) and cell mineralized deposit formation using Alizarin Red S (ARS) staining. In the in vivo studies, MTA and NPC were used to fill the rat molar perforations. Rat molars were processed at 7, 14 and 28 days for analysis of inflammatory processes using hematoxylin and eosin (HE) staining, immunohistochemical staining of Runx2 and tartrate-resistant acid phosphate (TRAP) staining. The results demonstrate that the nanoparticle size distribution of NPC is critical for osteogenic potential at an earlier stage compared to MTA. Further studies are required to elucidate the mechanism of action of NPC in osteogenic differentiation.

Keywords: tric.alcium silicate nanoparticle-containing cement (NPC); mineral trioxide aggregate (MTA); human periodontal ligament fibroblasts (HPLFs)

1. Introduction

One of the complications of root canal treatments is accidental perforation, and in particular, when the pulp chamber floor is perforated, the prognosis is often poor [1]. Our Department has compared and examined various perforation site sealants in order to improve the prognosis for perforations at the floor of the pulp chamber [2, 3].

When the floor of the pulp chamber is perforated, a calcium silicate-based cement, such as mineral trioxide aggregate (MTA), is generally used as a perforation sealant [4-6]. It has been reported that when MTA is co-cultured with human periodontal ligament cells, osteoprotegerin (OPG) and osteocalcin (OCN) mRNAs are expressed [7]. It has also been suggested that MTA promotes the differentiation of human periodontal ligament fibroblasts (HPLFs) into osteoblast/cementoblast-like cells [7]. However, MTA has a long setting time and is also difficult to manipulate and insert [5]. Moreover, there is evidence that bismuth oxide, used as a radiopacifier in dental materials, reduces compression resistance and inhibits cell proliferation [8, 9].

A tricalcium silicate nanoparticle-containing cement (NPC) was developed to overcome the disadvantages of existing MTAs [10, 11]. NPC has a superior operability independent of the dentist's skill, and its biocompatibility for a wide range of applications including endodontic repair and has attracted increasing attention in recent years as a cement designed as a bioactive dentin substitute, which has mechanical properties similar to dentin [10, 12, 13]. NPC has also been shown to have a faster setting time compared to MTA because the liquid contains calcium chloride and water-soluble polymers that reduce the time required for setting [10, 14, 15]. Many studies have been conducted in

Preprints (www.preprints.org) | NOT PEER-REVIEWED | Posted: 1 June 2023 doi:10.20944/preprints202306.0037.v1

the past comparing the effects of NPC on gene expression levels of runt-related transcription factor 2 (RUNX2) and receptor activator of nuclear factor-kappa B ligand (RANKL) to MTA in dental pulp cells [16-18]. However, studies on the effects of NPC on HPLFs are not completely clear. Therefore, the purpose of this study was to evaluate the effects of MTA and NPC in a rat model of pulp chamber floor perforation and in HPLFs.

2. Materials and Methods

In vitro studies

2.1. Cells

Commercially available primary HPLFs (ScienCell, #2630, San Diego, CA, USA) isolated from human periodontal tissue were used in this study.

2.2. Cell culture medium

Fibroblast Medium (FM), which is an HPLF growth medium (#2321, ScienCell, San Diego, CA, USA), was supplemented with 2% fetal bovine serum (FBS), fibroblast growth supplement (FGS-acf, #2372) and 1% antibiotic solution (P/S, #0503). The osteoinductive medium was prepared by adding dexamethasone (10^{-7}mol/L), ascorbic acid (2×10^{-4} mol/L) and glycerophosphate (10 mmol/L) to the FM.

2.3. Cell culture

HPLFs were seeded in 100-mm dishes at a density of 5,000 cells/cm^2 (275,000 cells/dish) and were cultured in FM that was changed every 3 days at a temperature of 37°C with 5% carbon dioxide. HPLFs were detached using trypsin/EDTA and were passaged. HPLFs that had reached confluence after 3-5 passages were used in this study. The day when the culture medium was changed is defined as day 0 (Figure 1).

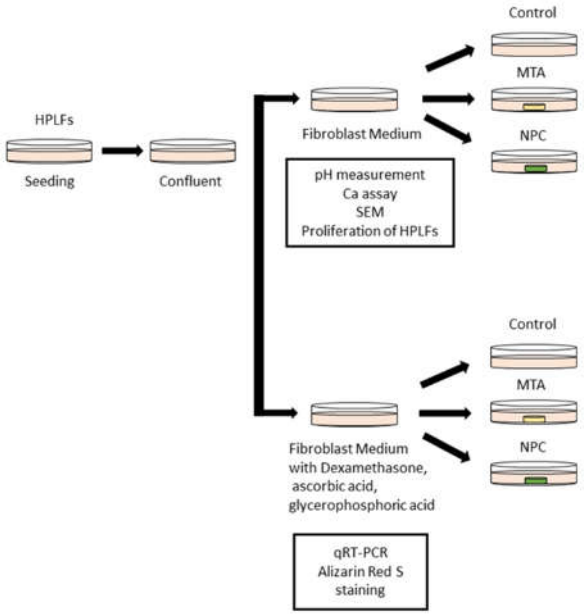

Figure 1. Schematic of the culture method of HPLFs used for the in vitro study. HPLFs were divided into two groups, one group was treated without Dexamethasone, ascorbic acid or glycerophosphoric acid while the other group was treated with Dexamethasone, ascorbic acid and glycerophosphoric acid.

Preprints (www.preprints.org) | NOT PEER-REVIEWED | Posted: 1 June 2023 doi:10.20944/preprints202306.0037.v1

2.4. Production of material disks containing MTA and NPC

The following tricalcium silicate-based cement materials were used to prepare extracts: (i) ProRoot® MTA (Dentsply Tulsa Dental Specialties, Tulsa, OK, USA) containing
Portland cement (tricalcium silicate, dicalcium silicate and tricalcium aluminate) 75%, calcium sulfate dihydrate (gypsum) 5% and bismuth oxide 20%, and (ii) Biodentine® (Septodont, Saint-Maur-des-Fossés, France) containing tricalcium silicate 80.1%, calcium carbonate 14.9% and zirconium oxide 5.0%.

MTA and NPC were obtained from dental material handling manufacturers. All cements were mixed according to the manufacturer's guidelines under aseptic conditions and were moulded into 7 mm diameter and 1 mm thickness disks. The sample size was estimated based on data from previous studies of similar design [19, 20]. All disks were placed in a 100% humidity incubator at 37°C for 24 h, then were immersed in 70% ethanol and sterilized with UV light for 30 min at room temperature. All disks were placed in the center of each well in 6-well plates.

2.5. pH measurement

A disk of each material in FM (pH 7.2, 2 mL) was placed in an atmospheric environment for 3 days. The pH of the medium was evaluated using a digital pH meter (LAQUA twin pH, HORIBA, Kyoto, Japan). As a control, FM was measured (n＝5).

2.6. Calcium ion release

Calcium ion release from the materials was measured in the presence or absence of HPLFs. HPLFs (5.0×10^4) were seeded in 6-well culture plates in a 100% humidity incubator at 37°C for 3 days. After day 3, the concentration of calcium ions in the medium was measured. Calcium ion release was measured using a calcium assay kit (Metallogenics, Chiba, Japan). Calcium ion release in the medium was rapidly quantified in a microplate reader (96 wells) and the calcium ion concentration was calculated. As a control, FM was measured in the presence or absence of HPLFs (n = 5).

2.7. Scanning electron microscope (SEM) observations

Observations of material particle size, disk surface morphology and cell adhesion were performed using a SEM (Hitachi S-4800, Hitachi High-Technologies Corp., Tokyo, Japan) (at 1.00k × magnification, 15 kV). Disks made of each material were placed in 6-well plates and HPLFs (1.0×10^6) were seeded on those disks and cultured in a 100% humidity incubator at 37°C for 3, 6, 10 and 14 days. After the incubation period, the material disks along with cells growing on their surfaces, were washed twice with PBS and were fixed overnight in Karnovsky's fixative (2.5% glutaraldehyde, 2% formaldehyde, 0.1M sodium cacodylate). The disks were then dehydrated in a graded series of ethanol (70%–95% v/v), mounted on a sample stage and coated with gold/palladium prior to SEM observation (n = 5).

2.8. Proliferation of HPLFs

HPLFs (5.0×10^4 cells) were seeded in 6-well plates and then exposed to each type of cement in a 100% humidity incubator at 37°C. At days 1, 3 and 5, cell proliferation was evaluated using a Coulter Counter (Beckman Coulter, Tokyo, Japan) and the numbers of cells were calculated. As a control, cells were not exposed to any cement (n = 5). The FM was changed every 3 days.

2.9. Quantitative reverse transcription polymerase chain reaction (qRT-PCR)

HPLFs that had been seeded in osteoinductive medium at days 3 and 6 in each group were collected. Total RNAs were extracted using a RNeasy Mini Kit (QIAGEN, Hilden, Germany) and were reverse transcribed into complementary DNAs (cDNAs) using ReverTra Ace qPCR RT Master Mix with gDNA Remover (TOYOBO, Osaka, Japan). qRT-PCR was performed using TaqMan Gene Expression Assays (Applied Biosystems, Waltham, MA, USA). The target genes characterized in this study as osteoblast markers were: RUNX2 mRNA (Hs01047973-m1), OCN mRNA (Hs01587814-g1),

Preprints (www.preprints.org) | NOT PEER-REVIEWED | Posted: 1 June 2023 doi:10.20944/preprints202306.0037.v1

RANKL mRNA (Hs00243522-m1) and OPG mRNA (Hs00900358-m1). Glyceraldehyde-3-phosphate dehydrogenase (GAPDH: Hs02786624_g1) was used as an endogenous control. qRT-PCR was performed using a 7500 Fast Real-Time PCR System (Applied Biosystems, Waltham, MA, USA). mRNA expression levels were corrected based on GAPDH mRNA expression levels, and target gene expression levels were subjected to relative quantitative analysis. As a control, osteoinductive medium was measured in the presence of HPLFs (n = 5).

2.10. Alizarin Red S (ARS) staining

ARS staining was used to assess mineralized deposit formation in cell cultures. The purpose of carrying out ARS staining is to quantitatively evaluate the amount of calcium deposited by the calcium silicate cement. HPLFs (1.0×10^6) were seeded in osteoinductive medium (2 mL) in 6-well culture plates containing material disks (n = 5) for 24 days. The osteoinductive medium was changed every 3 days. After day 24, HPLFs were fixed with 2% paraformaldehyde (Nacalai Tesque, Inc, Kyoto, Japan) for 10 min at room temperature. After fixation, each well was washed twice with purified water and 1 mL ARS staining solution (pH 6.4) was added. After standing at room temperature for 10 min, the ARS staining solution was aspirated from the wells, and the wells were washed 3 times with purified water (1 mL each). The wells were photographed immediately after drying in air (Canon Inc., Tokyo, Japan). Results were analyzed statistically by measuring the stained area within each photograph.

In vivo studies

2.11. Experimental design

The study protocol complied with the Guidelines for the Treatment of Experimental Animals at Tokyo Dental College (Approval Number: 200502). In this study, 36 healthy male Wistar rats, 10 weeks old and each weighing an average of 300 g (Sankyo Lab Service, Tokyo, Japan), were used. The animals were in good health at the beginning of the experiment.

The sample size was estimated based on data from previous studies of similar design [21]. Using an alpha error of 0.05% and 95% power to recognize a significant difference of 1 in the median scores, a minimum of 9 animals per group was considered necessary. Taking into consideration the possible complications that could occur during the study, one more animal was added in each group for each experimental time. Considering three observation times, 36 animals were necessary. Rats were anesthetized using three kinds of mixed anesthesia (1.5 ml/mg, Domitor (ZENOAQ, Fukushima, Japan), Midazolam (SANDOZ, Tokyo, Japan) and Butorphanol (Meiji Seika, Tokyo, Japan)). Perforation of the pulp chamber floor was performed according to the method described by Nakauchi et al. [22]. Briefly, a cavity was prepared on the occlusal surface of the upper first molar of each rat using a 0.5 mm round burr (MANI#1/4, INC, Tochigi, Japan). The pulp chamber floor was then perforated toward the periodontal ligament (PDL) without injuring the alveolar bone. The perforation was confirmed using a stereoscopic microscope. The coronal access was performed at low speed with saline solution irrigation. Hemorrhages were arrested using physiological saline irrigation and sterile cotton pellets. All materials were gently placed with a curette until they completely filled the furcation perforation (shown schematically in Figure 2A). After the initial setting time, all coronal access cavities were restored with a light-curing glass ionomer cement (GIC, DMG, Chemisch-Pharmazeutische Fabrik GmbH, Berlin, Germany). At the end of the experimental period, rats were euthanized by an anesthetic overdose. During the experiment, all rats were housed under a 12-h light / 12-h dark cycle at a controlled temperature (22°C), with water and food provided ad libitum. The general health of rats was monitored throughout the experimental period. The groups were divided into three groups of each material at 7, 14 and 28 days (Control, MTA and NPC groups). The control group was GIC only (n=4).

Preprints (www.preprints.org) | NOT PEER-REVIEWED | Posted: 1 June 2023 doi:10.20944/preprints202306.0037.v1

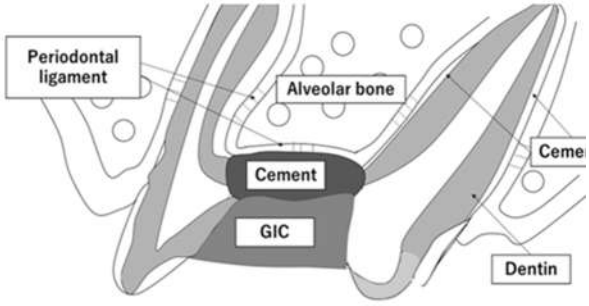

(A) The pulp chamber floor was perforated toward the PDL without injuring the alveolar bone using a 0.5 mm round burr. The perforations were filled with one of the cements. After the initial setting time, all coronal access cavities were restored with GIC.

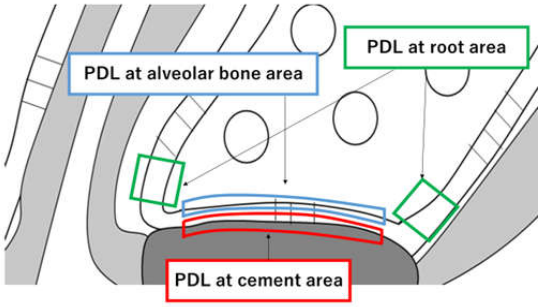

(B) Three observation areas. PDL at the cement areas; PDL at the furcation area attached to the cement; PDL at the root areas; PDL at the coronal side of the tooth root (100 μm x 100 μm). PDL at the alveolar bone area; PDL at furcation area attached to the alveolar bone ridge.

Figure 2. Experimental design of the in vivo study.

2.12. Histological observations

At days 7, 14 and 28 after surgery, the maxillary first molar of each rat was excised together with the maxillary bone. The excised maxilla was immersed and fixed in 4% paraformaldehyde at 4°C for 24 h, decalcified with 10% EDTA (Fuji Film, Tokyo, Japan) at 4°C for 1 month, and then embedded in paraffin. The EDTA was changed 3 times a week. Paraffin blocks were sectioned approximately 5 μm thick sagittally to the tooth. After sectioning, the sections were deparaffinized and stained with hematoxylin and eosin (HE). We observed three areas: the PDL at cement areas, the PDL at root areas and the PDL at alveolar bone areas. The PDL at cement areas shows the PDL at the furcation area attached to the cement. The PDL at root areas shows the PDL at the coronal side of the tooth root. The PDL at alveolar bone areas shows the PDL at furcation area attached to the alveolar bone ridge (Figure 2B).

2.13. Immunohistochemical staining of Runx2, and ratio of Runx2-positive cells

For immunohistochemical observations, the paraffin sections were deparaffinized with xylol, after which they were activated for antigen using by a tryptic antigen retrieval kit (Abcam, Cambridge, UK) for 10 min. Each section was immersed in methanol containing 0.3% aqueous hydrogen peroxide at room temperature to block endogenous peroxidase activity, then blocked for 30 min with 10% goat serum at room temperature to reduce non-specific binding. Sections were reacted with the primary antibody overnight at 4°C. The primary antibody used was Runx2 (sc-390351, 1:50; Santa Cruz Biotechnology, Dallas, TX, USA). The sections were then reacted with MACH 2 Universal HRP Polymer Detection (BRR522G, BIOCARE MEDICAL, Pacheco, CA, USA) as a peroxidase-conjugated secondary antibody for 30 min at room temperature, after which they were stained with 3,3'-diaminobenzidine (DAB), and nuclei were stained with hematoxylin. As a negative control, the primary antibody was replaced with goat nonimmune serum. The PDL at the root area (100 μm x 100 μm) as shown in Figure 2B was observed with a light microscope and the number of Runx2-positive cells was counted. The ratio of Runx2-positive cells was calculated as Runx2-positive cells/total cells × 100 (%).

2.14. Tartrate-resistant acid phosphate (TRAP)-positive staining, and the number of TRAP-positive cells

The histochemical TRAP reaction was used as an osteoclast marker (Fuji Film, Tokyo, Japan). After deparaffinization and washing with water, the TRAP staining solution (0.5 ml, pre-adjusted) was incubated on each section for 30 min at room temperature, after which they were washed in distilled water, counterstained with hematoxylin, and mounted in aqueous medium. The number of TRAP-positive cells was determined as previously described [23, 24]. TRAP-positive cells were

Preprints (www.preprints.org) | NOT PEER-REVIEWED | Posted: 1 June 2023 doi:10.20944/preprints202306.0037.v1

counted within the PDL at alveolar bone areas corresponding in length to the perforation area (Figure 2B). In each section, an image of the interradicular alveolar process was captured using a camera attached to a light microscope. Subsequently, the numbers of multinucleated TRAP-positive cells adjacent to the alveolar process surface were counted using a light microscope and were divided by the total length of the bone perforation surface [21].

2.15. Statistical analysis

Quantitative data are expressed as means ± standard deviation (SD) using GraphPad Prism7 (MDF Corp., Tokyo, Japan). Quantitative data were analyzed by relative evaluation using Student's t-test and one-way ANOVA analysis with post hoc Tukey's multiple comparisons test (* $p < 0.05$).

3. Results

In vitro studies

3.1. pH measurement

The mean values and standard deviations of pH observed for each type of cement tested are shown in Table 1. The control pH was 8.28 ± 0.01, the MTA pH was 8.88 ± 0.01, and the NPC pH was 8.82 ± 0.00. The pH values of the MTA and NPC groups were higher than the control group. There was no significant difference between the MTA and NPC groups.

Table 1. Mean pH values for control, MTA and NPC over 3 days. The pH values of the MTA and NPC groups were higher than those of the control group (* $p < 0.0001$). There was no significant difference between the MTA and NPC groups (n=5).

pH (Day 3)	
Group	**Mean ± SD**
Control	8.28 ± 0.01
MTA	8.88 ± 0.01 *
NPC	8.82 ± 0.00 *

3.2. Calcium release

In the absence of HPLFs, calcium ion levels in the NPC group were significantly higher than in the control and MTA groups (Figure 3). In the presence of HPLFs, the calcium ion levels in the MTA and NPC groups were significantly higher than in the control group, and there were no significant differences between the MTA and NPC groups. Interestingly, calcium ion levels in the presence of HPLFs were significantly reduced in the NPC group compared to calcium ion levels in the absence of HPLFs.

Preprints (www.preprints.org) | NOT PEER-REVIEWED | Posted: 1 June 2023 doi:10.20944/preprints202306.0037.v1

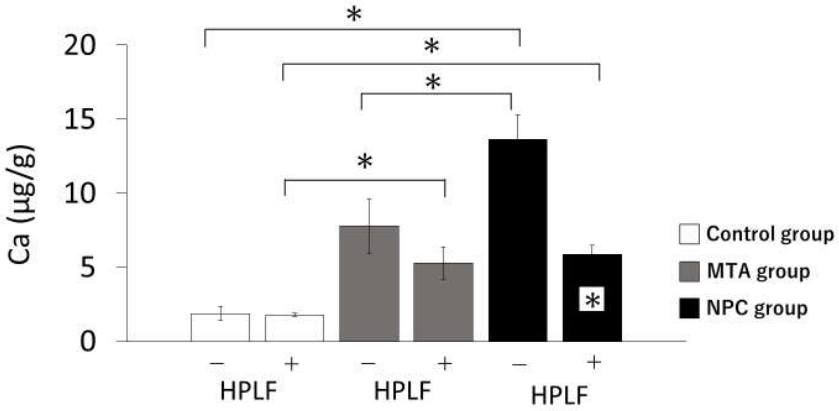

Figure 3. Mean values of calcium ion release from the control, MTA and NPC groups over 3 days. The + at the bottom of the graph indicates the presence of HPLFs and the - indicates the absence of HPLFs. Asterisks in the bars indicate significant differences between the materials. In the absence of HPLFs, the amount of calcium ions released in the NPC group was significantly higher than in the control and MTA groups. In the presence of HPLFs, both the MTA and NPC groups released significantly higher amounts of calcium ions than the control group, and there were no significant differences between the MTA and NPC groups. Calcium ion levels in the presence of HPLFs were significantly reduced in the NPC group compared to calcium ions in the absence of HPLFs (* $p < 0.05$).

3.3. SEM analysis

MTA and NPC particles had uneven shapes (Figure 4A, B). In addition, the MTA and NPC disk surfaces had uneven shapes, and the MTA granules had a round shape while the NPC granules had a square shape. HPLFs that attached on each experimental disk at day 3 were similar with a spindle shape (Figure 4C, D). HPLFs that attached on each experimental disk at day 6 showed multiple process extensions in the NPC group compared to the MTA group (Figure 4E, F). At days 10 and 14, HPLFs were observed to overlap in multiple layers on the disk surface of both types of cement (Figure 4G–J).

Preprints (www.preprints.org) | NOT PEER-REVIEWED | Posted: 1 June 2023 doi:10.20944/preprints202306.0037.v1

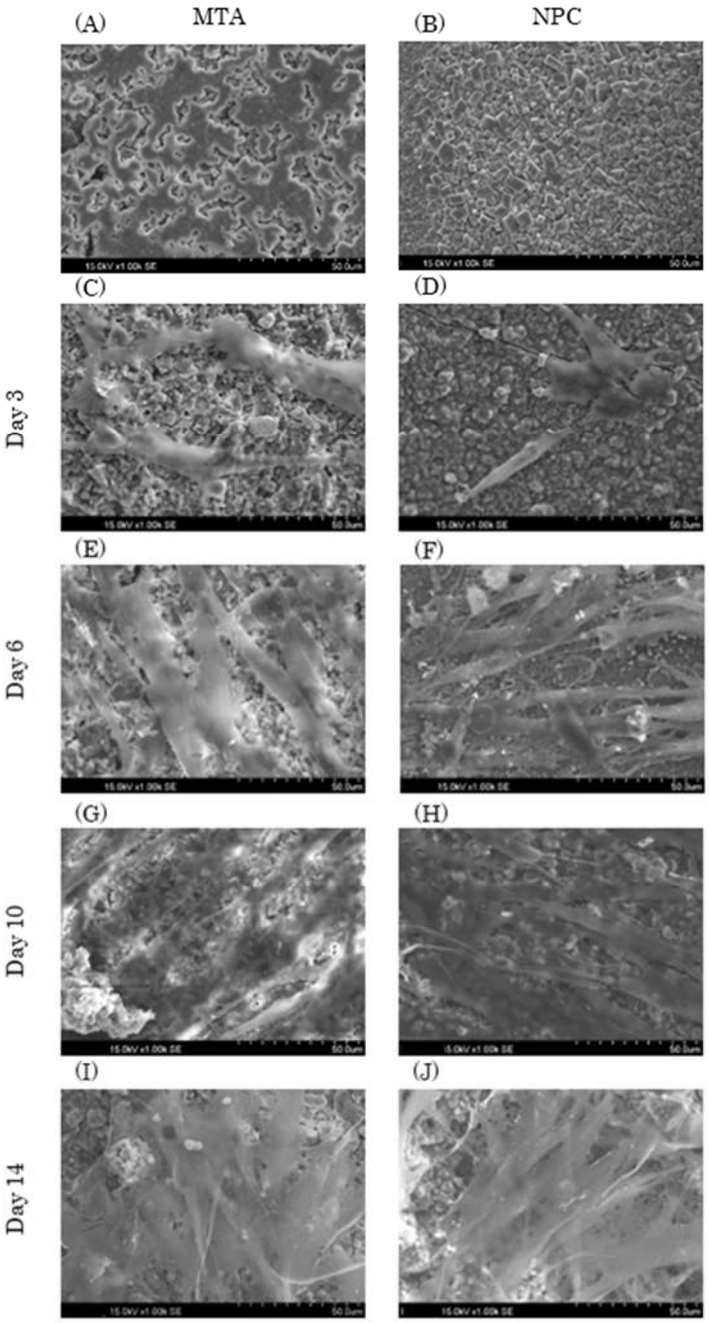

Figure 4. Representative SEM images of MTA and NPC with HPLFs (1.00k × magnification). HPLFs were seeded directly on top of the solid material disks. (A, B) Each experimental disk without HPLFs. The left column shows images of MTA disks with HPLFs seeded at days 3 (C), 6 (E), 10 (G), and 14 (I), and the right column shows images of NPC disks with HPLFs seeded at days 3 (D), 6 (F), 10 (H), and 14 (J).

3.4. Proliferation of HPLFs

HPLFs exposed to MTA or NPC showed proliferation rates that were statistically similar to the control (Figure 5). A significant increase in proliferation was observed in the MTA group compared to the control group at day 5.

Preprints (www.preprints.org) | NOT PEER-REVIEWED | Posted: 1 June 2023 doi:10.20944/preprints202306.0037.v1

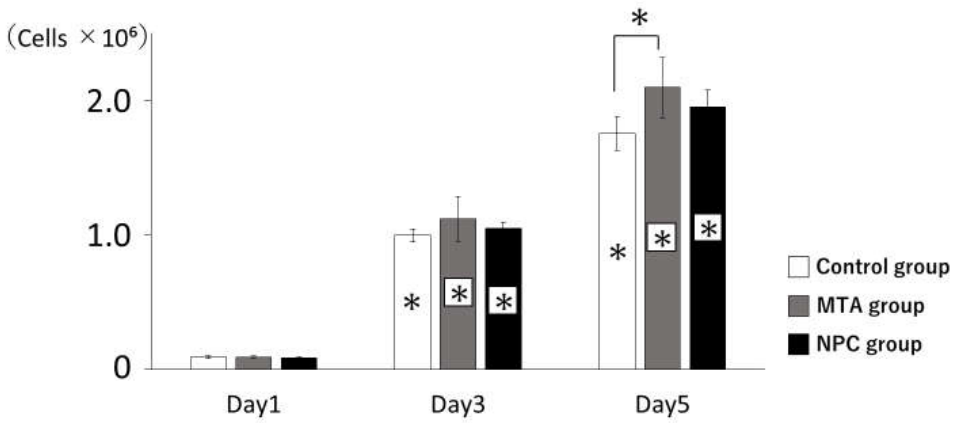

Figure 5. Proliferation of HPLFs. The number of HPLFs at days 3 and 5 showed significantly higher viability rates than at day 1. All groups had higher viability rates from day 1 to day 5. There were no significant differences among the three groups at days 1 through 3. The number of HPLFs in the MTA group was significantly higher than in the control group at day 5 (* $p < 0.05$).

3.5. qRT-PCR

The mRNA expression level of RUNX2 was significantly higher in the MTA and NPC groups at day 6 compared to the MTA and NPC groups at day 3 (Figure 6A). Although in the period of 3 days, there was an increase in the expression of OCN mRNA in the MTA and NPC groups, this higher level was statistically significant only at day 6. Furthermore, the mRNA expression level of OCN in the NPC group was significantly higher than in the MTA group at day 6 (Figure 6B). The mRNA expression level of RANKL was significantly lower in the MTA group at day 3 compared to the control group. However, the mRNA expression level of RANKL at day 6 was not significantly different among the three groups at day 6 (Figure 6C). The mRNA expression level of OPG was significantly higher in the NPC group at day 6 compared to the NPC group at day 3. The mRNA expression level of OPG at days 3 and 6 was not significantly different among the three groups (Figure 6D).

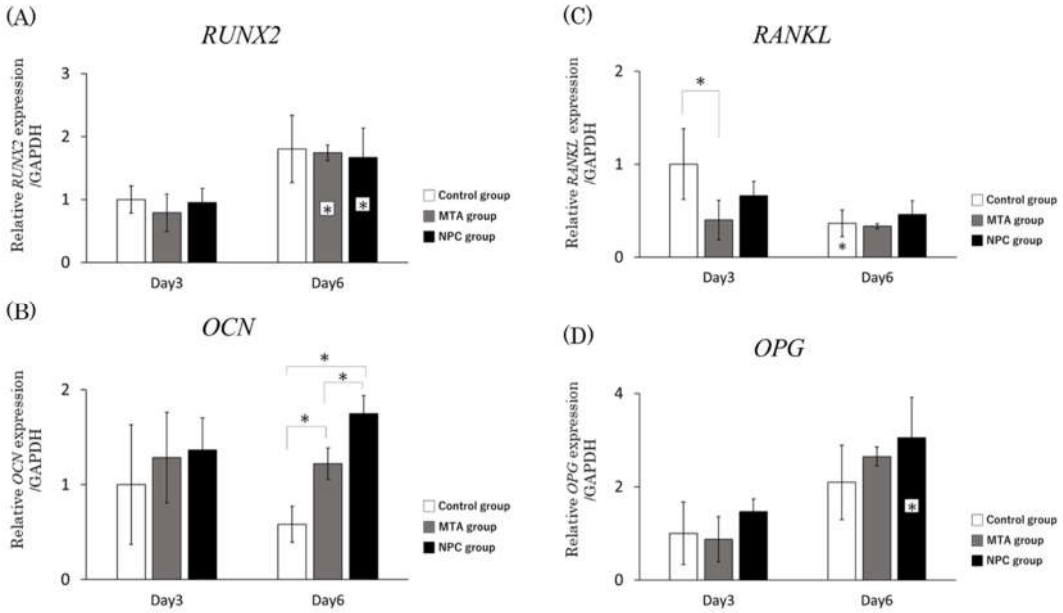

Figure 6. qRT-PCR analysis showed that the mRNA expression levels of HPLFs in vitro were as follows. Asterisks in the bars indicate significant differences between the same materials compared to day 3. (A) 2 mRNA expression levels at day 6 were significantly higher than at day 3 in the MTA group. RUNX2 mRNA expression levels at day 6 were significantly higher than at day 3 in the NPC group. (B) OCN mRNA expression levels in the MTA group were significantly higher than in the control group at day 6. Furthermore, it was significantly

Preprints (www.preprints.org) | NOT PEER-REVIEWED | Posted: 1 June 2023 doi:10.20944/preprints202306.0037.v1

higher in the NPC group than in the control and MTA groups at day 6. (C) RANKL mRNA expression levels in the MTA group were significantly lower than in the control group at day 3. RANKL mRNA expression levels at day 6 were significantly lower than at day 3 in the control group. There were no significant differences between the MTA and NPC groups at days 3 and 6. (D) OPG mRNA expression levels at day 6 were significantly higher than at day 3 in the NPC group. There were no significant differences among the three groups on either day 3 or day 6 (* $p < 0.05$).

3.6. Mineralization and ARS staining analysis

After 24 days of HPLF culture on the different materials in osteogenic medium, the MTA and NPC groups had increased amounts of calcium deposits (Figure 7A). In particular, the NPC group produced significantly more calcified deposits than the control group and the MTA group (Figure 7B).

3.6. Mineralization and ARS staining analysis

After day 24 of HPLF culture on the different materials in osteogenic medium, the MTA and NPC groups had increased amounts of calcium deposits (Fig. 7A). In particular, the NPC group produced significantly more calcified deposits than the control group and the MTA group (Fig. 7B).

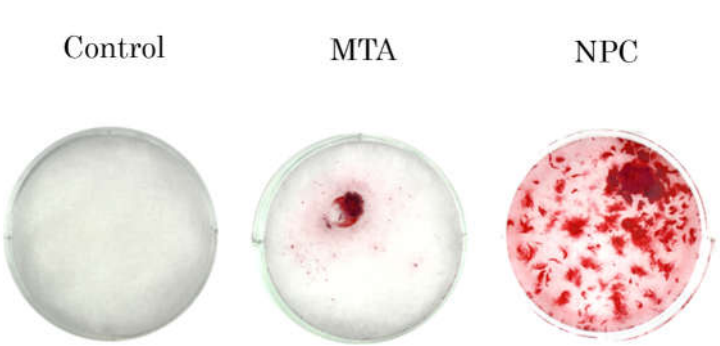

(A) Representative images of ARS staining assay.

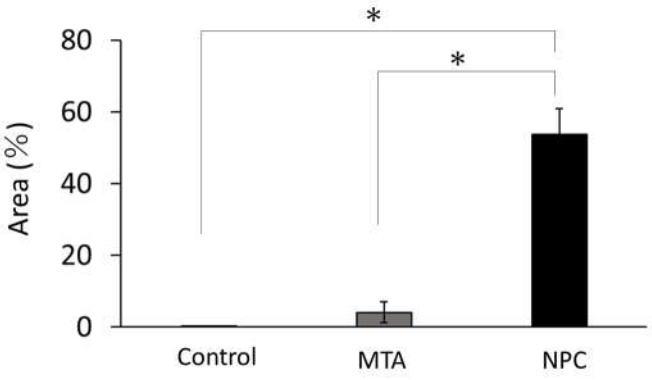

(B) ARS activity of the MTA and NPC media. In particular, the NPC group produced significantly more calcified deposits than the control group and the MTA group (* $p < 0.05$).

Figure 7. ARS staining assay of MTA and NPC media at day 24.

3.7. Histological observations

At day 7, inflammatory cell infiltrations and multinucleated giant cells were observed in the control group (Figure 8A). Inflammatory cells and a few osteoblasts were observed in the MTA and NPC groups (Figure 8B, C). At day 14, inflammatory cells, multinucleated giant cells and epithelial layers were observed in the control group (Figure 9A). A small number of inflammatory cells and a line of osteoblasts were observed in the MTA and NPC groups (Figure 9B, C). At day 28, a small number of inflammatory cells, osteoblasts and epithelial layers were observed in the control group (Figure 10A). A few inflammatory cells and a line of osteoblasts were observed in the MTA and NPC groups (Figure 10B, C). No epithelial layer was observed in the MTA and NPC groups.

Preprints (www.preprints.org) | NOT PEER-REVIEWED | Posted: 1 June 2023 doi:10.20944/preprints202306.0037.v1

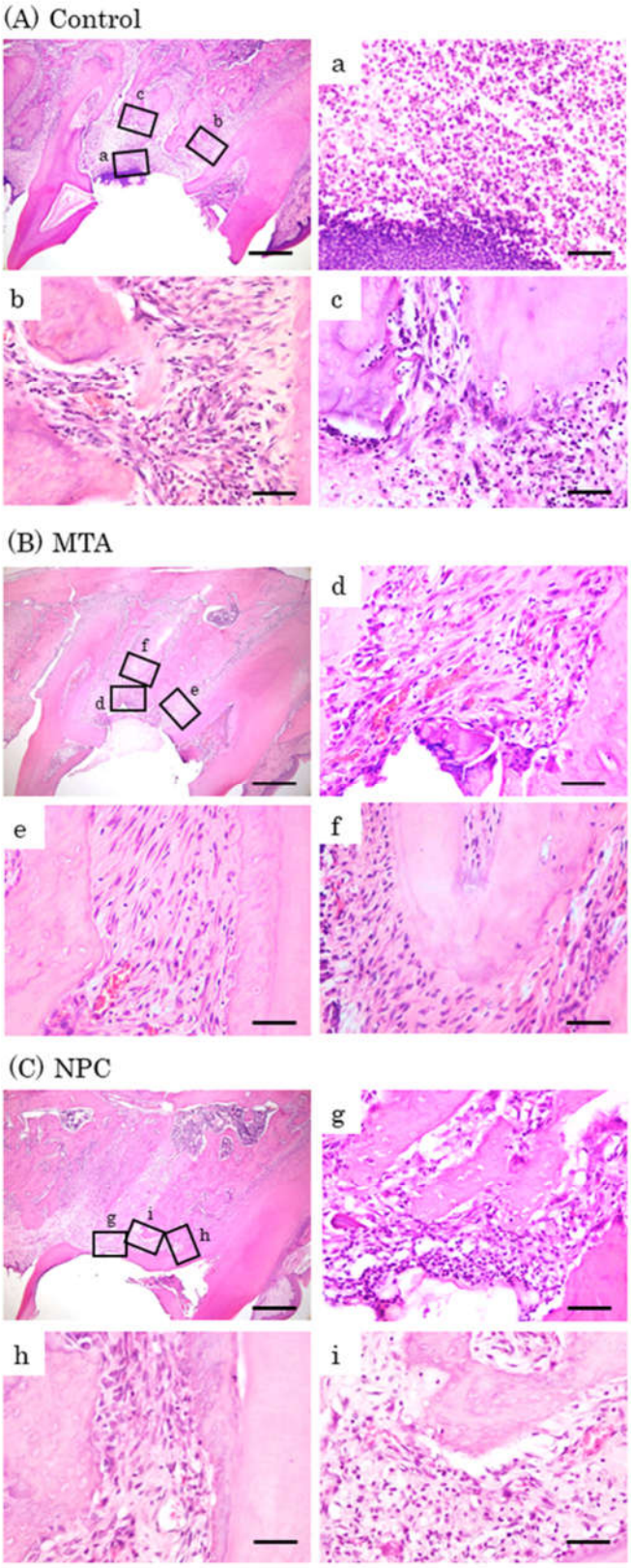

Figure 8. Representative features in the in vivo study using HE staining after surgery at day 7. Light micrographs of sagittal sections of maxilla showing the first molars of the control (A), the MTA (B) and the NPC (C) groups. (A) Numerous inflammatory cells (a–c), and multinucleated giant cells were observed (c). (B, C) Inflammatory cells (d, f, g, i), and a small number of osteoblasts were observed (e, h). Scale bars: 500 micrometers; a–i: 50 micrometers.

Preprints (www.preprints.org) | NOT PEER-REVIEWED | Posted: 1 June 2023 doi:10.20944/preprints202306.0037.v1

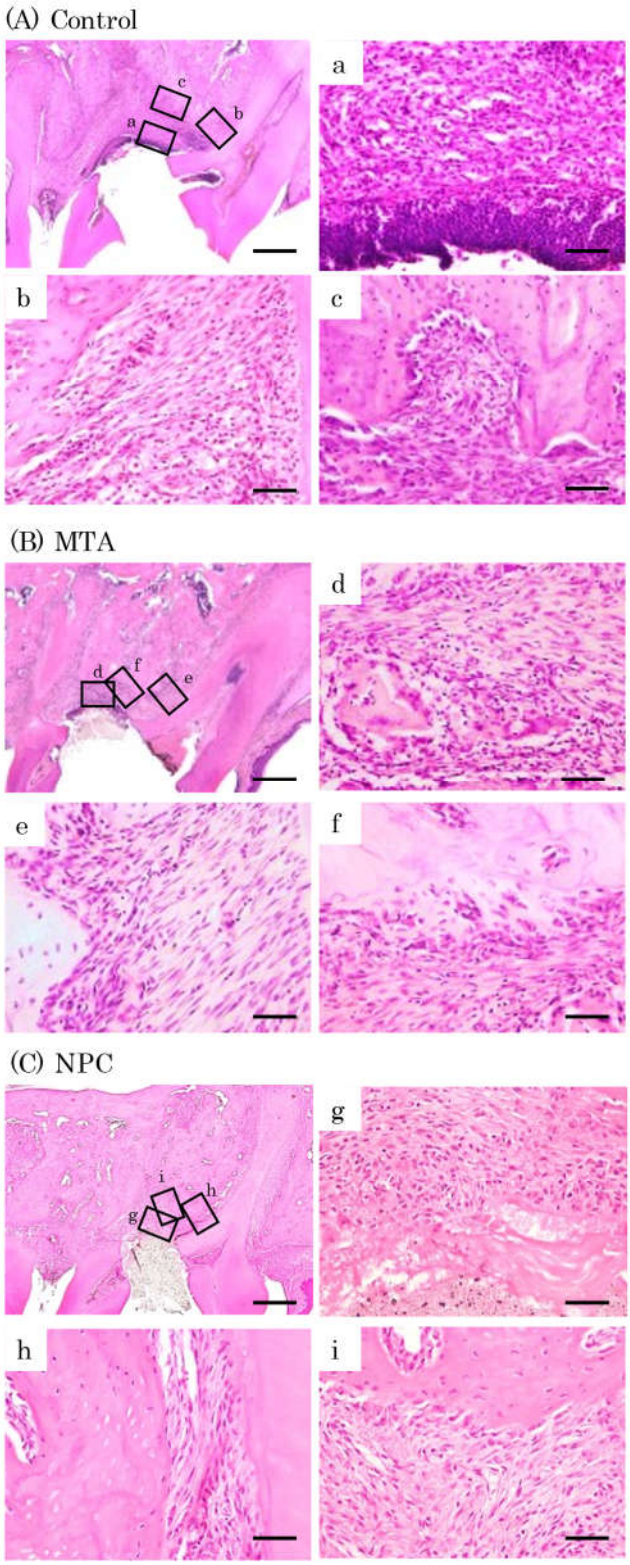

Figure 9. Representative features in the in vivo study using HE staining after surgery at day 14. Light micrographs of sagittal sections of maxilla showing the first molars of the control (A), the MTA (B) and the NPC (C) groups. (A) An epithelial layer, numerous inflammatory cells (a–c), and multinucleated giant cells were observed (c). (B, C) A small number of inflammatory cells (d, f, g, i), and a line of osteoblasts were observed (e, f, h, i). Scale bars: 500 micrometers; a–i: 50 micrometers.

Preprints (www.preprints.org) | NOT PEER-REVIEWED | Posted: 1 June 2023 doi:10.20944/preprints202306.0037.v1

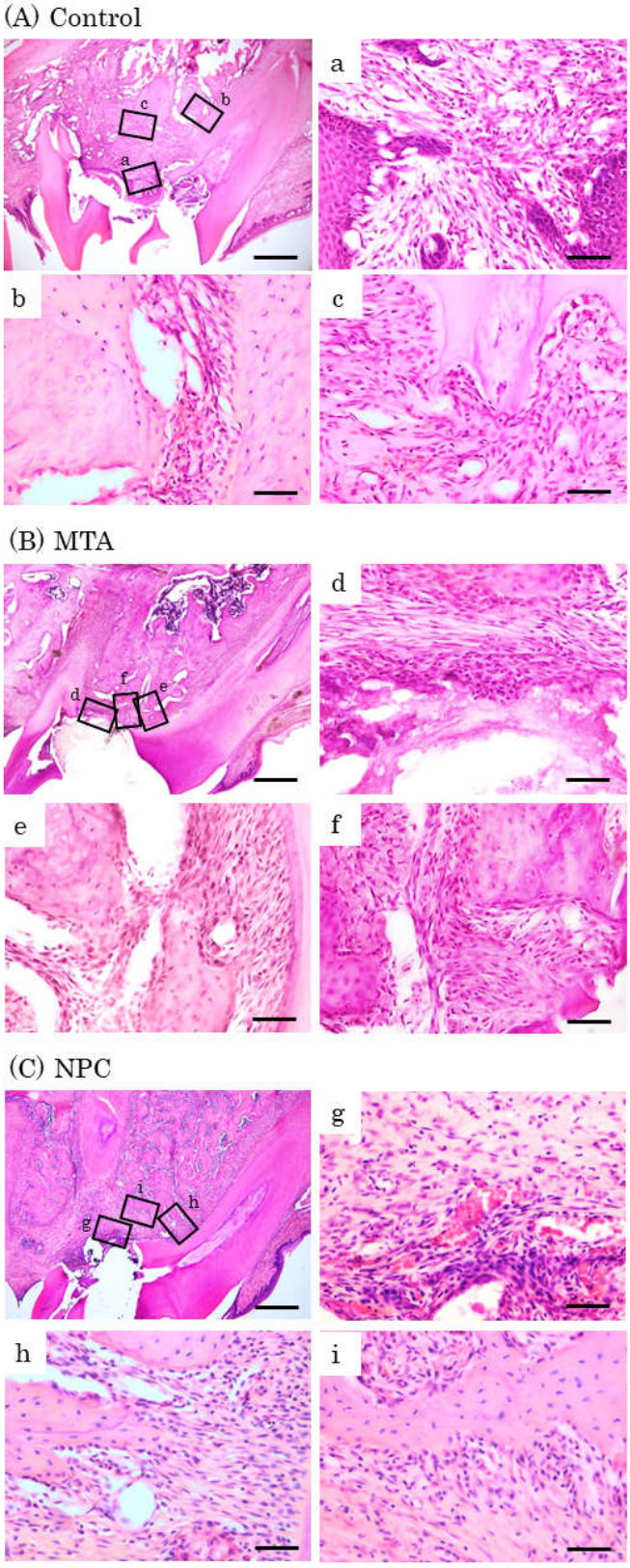

Figure 10. Representative features in the in vivo study using HE staining after surgery at day 28. Light micrographs of sagittal sections of maxilla showing the first molars of the control (A), the MTA (B) and the NPC (C) groups. (A) An epithelial layer, a small number of inflammatory cells (a–c), and osteoblasts (b, c). (B, C) A few inflammatory cells (d, g), and a line of osteoblasts were observed (e, f, h, i). Scale bars: 500 micrometers; a–i: 50 micrometers.

Preprints (www.preprints.org) | NOT PEER-REVIEWED | Posted: 1 June 2023 doi:10.20944/preprints202306.0037.v1

3.8. Immunohistochemical observations of Runx2, and the ratio of Runx2-positive cells

At day 7, Runx2-positive cells were observed in the NPC group, but not in the control or MTA groups (Figure 11A–C). At days 14 and 28, a small number of Runx2-positive cells was observed in the control group and numerous Runx2-positive cells were observed in the MTA and NPC groups (Figure 11D–I). Quantitative analysis revealed that the number of Runx2-positive cells was highest in the NPC group and significant differences were observed between the MTA and NPC groups, at day 14 (Figure 12J). Furthermore, significant differences were observed between the control and NPC group, at all time points.

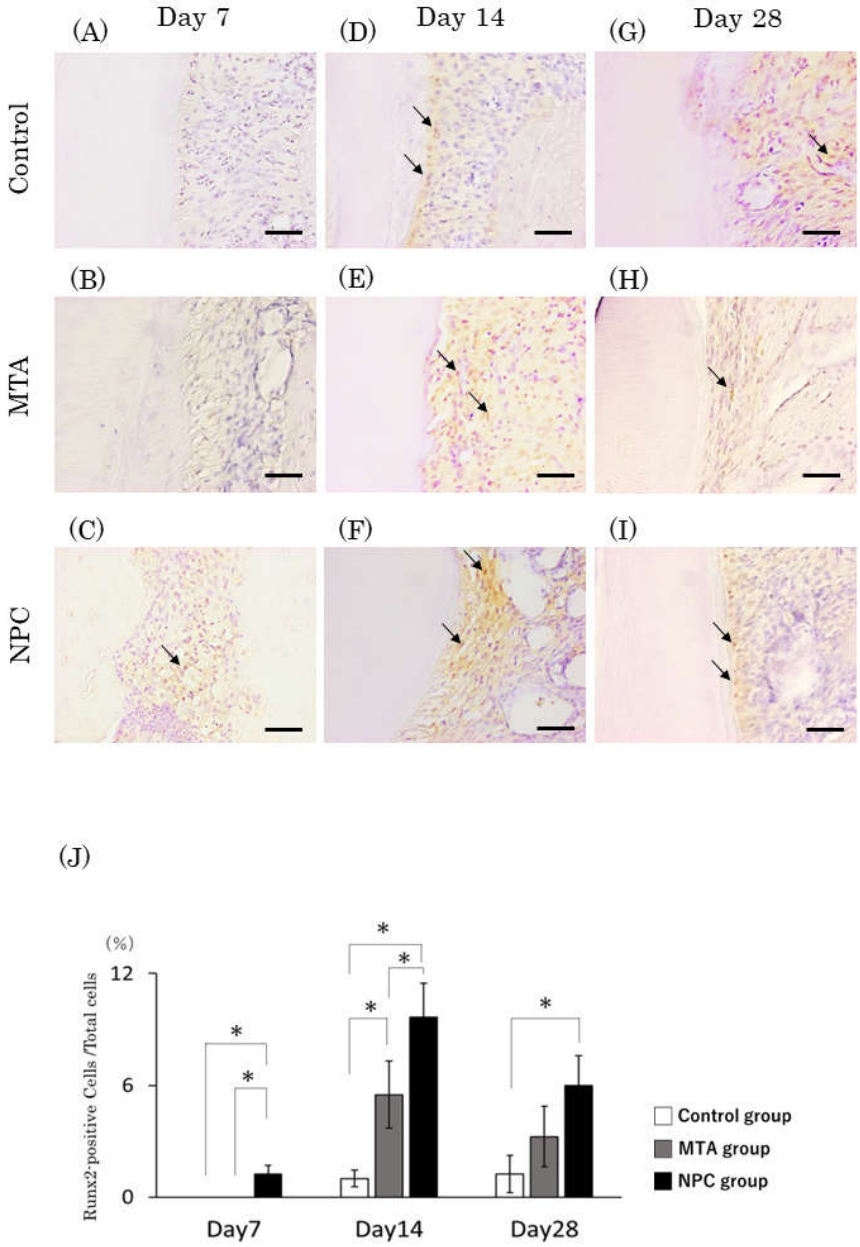

Figure 11. Immunohistochemical staining of Runx2. Light micrographs of sagittal sections of the PDL at root areas of the control (A, D, G), the MTA (B, E, H) and the NPC (C, F, I) groups at day 7 (A–C), at day 14 (D–F) and at day 28 (G–I). (A–C) Runx2-positive cells were not observed in the PDL of the control or the MTA groups while evident Runx2-positive cells were present in the NPC group. (D–I) Several Runx2-positive cells were observed in the PDL of all groups. (J) Graph showing the number of Runx2-positive cells in the PDL at root areas from the control, MTA and NPC groups at days 7, 14 and 28. The highest number of Runx2-positive cells was found in the NPC group. The number of Runx2-positive cells at days 7 and 14 was significantly higher in the

Preprints (www.preprints.org) | NOT PEER-REVIEWED | Posted: 1 June 2023 doi:10.20944/preprints202306.0037.v1

NPC group than in the control and MTA groups; at day 28, the NPC group was significantly higher than the control group, but was not significantly different from the MTA group (* $p < 0.05$). Arrows; Runx2-positive cells. Scale bars: 50 micrometers.

3.9. Observations of TRAP staining and the number of TRAP-positive cells

At day 7, numerous TRAP-positive cells were observed in the control group and a small number of TRAP-positive cells were observed in the MTA and NPC groups (Figure 12A–C). At day 28, an apparent reduction in the number of TRAP-positive cells was seen in the control group (Figure 12D) while a small number of TRAP-positive cells was observed in the MTA and NPC groups (Figure 12E, F). Quantitative analysis revealed that the highest number of TRAP-positive cells was seen in the control group and no significant differences were observed between the MTA and NPC groups, at any time point (Figure 12G). At day 28, the number of TRAP-positive cells decreased significantly in the control group compared to day 7.

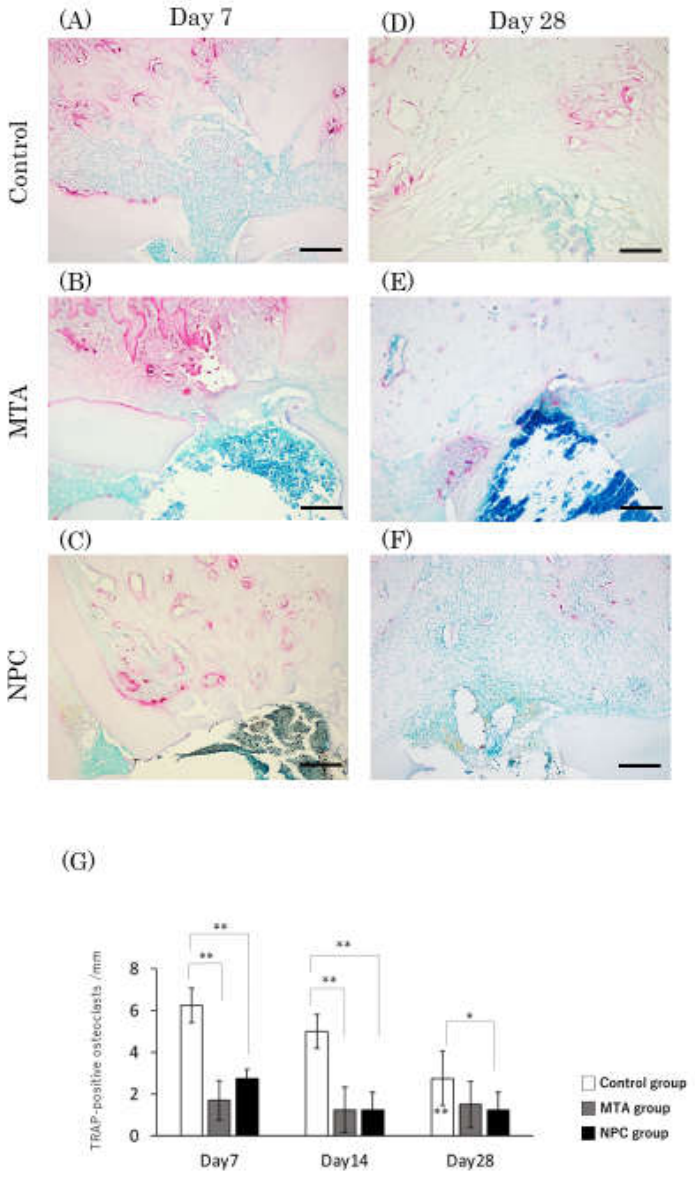

Figure 12. Light micrographs of sagittal sections of the PDL at alveolar bone areas of the control (A, D), the MTA (B, E) and the NPC (C, F) groups at day 7 (A–C) and at day 28 (D–F). (A–C) Several TRAP-positive cells were present in the periodontal space adjacent to the surface of the alveolar process next to the perforated pulp chamber floors. (D–F) Few TRAP-positive cells were adjacent to the bone surface of any

 doi:10.20944/preprints202306.0037.v1

group. (G) Graph showing the number of TRAP-positive cells in the PDL at alveolar bone areas from the control, MTA and NPC groups at days 7, 14 and 28. Asterisks in the bars indicate significant differences between the same materials compared to day 7. The highest number of osteoclasts was found in the control group while no significant differences were observed between the NPC and the MTA groups at any time point. In the control group, no significant differences were detected from day 7 to 14, but from day 7 to 28, a significant reduction in the number of TRAP-positive cells were observed (* $p < 0.05$). Scale bars: 200 micrometers.

4. Discussion

NPC has a superior operability and biocompatibility compared with MTA and has been reported to be the best material for clinical applications such as pulp capping, perforation repair, apexification and reverse root canal filling [10]. NPC also has the advantage of a very short setting time compared to MTA [14]. Furthermore, it has been reported that using NPC as a reverse root canal filling material significantly increased calcium and silicic acid uptake into dentin compared to MTA [23]. ZrO_2 in NPC has been reported to improve biocompatibility [25]. However, most research on NPC has been conducted in an in vitro environment, and there are very few in vivo studies.

In our in vitro study, HPLFs were seeded around the disks, not just on the disks, because in clinical treatments, the effects act on areas that are not in direct contact with the material. In the in vivo study, the material affects HPLFs through the interstitial fluid, so we observed and evaluated areas in contact with or not in contact with the material.

The calcium ion concentration in the medium showed the highest value in the NPC group. Similarly, ARS staining revealed that the NPC group produced significantly more calcified deposits than the MTA group. Previous studies investigating cell proliferation and calcification have reported that extracellular alkaline conditions promote proliferation and calcification of human cementoblasts in vitro [26]. It has been suggested that NPC should be kneaded with calcium chloride, which increases the proportion of calcium compared to MTA and results in an increase in calcium ion concentration [27]. Calcium silicate has been reported to cause a highly alkaline environment and to increase the influx of calcium ions into the extracellular environment [28]. It has also been reported that the hydration of NPC produces more calcium than MTA, speeding up the rate of calcification and new bone growth [23]. Calcium chloride promotes hydration reactions and calcium phosphate deposition while maintaining a high pH [29]. These results indicate that the high pH environment and Ca leaching brought about by NPC affects calcification [20]. These results are also consistent with previous studies showing that calcium silicate-based cements induce calcification [19, 30, 31]. On the other hand, MTA and NPC have been reported to have an initial cytotoxicity due to the highly alkaline environment and to cause an initial inhibitory effect on cell growth [12]. In this study, cytotoxicity was evaluated by characterizing the cell proliferation rate. All groups had higher viability rates from days 1 to 5, which suggests that MTA and NPC are not cytotoxic. Furthermore, our in vivo experiments showed that the PDL of the MTA and NPC groups showed a decrease in inflammatory cells with an increase in osteoblasts.

In addition to the HPLF proliferation rate assay, SEM images were acquired to evaluate the physical appearance of HPLFs growing in direct contact on the disks. NPC powder components were previously analyzed using a particle size analyzer. It has been reported that nano-sized particles were detected from a study using a particle size analyzer [11]. Incorporating nanoparticles into the powder component may increase the surface area and ionization, which is considered to reduce the setting time [11]. It has also been reported that calcium plays an important role in fibroblast adhesion and that a higher percentage of calcium may result in better cell adhesion [30, 31]. The results of this study show that the cell morphology of HPLFs that adhered to NPC disks had a typical spindle-shaped morphology with more spreading cell projections and cell body extensions, compared to the MTA group. We speculate that this result is due to the fact that NPC contains nanoparticles, which increases the surface area of the disks compared to MTA, allowing cells to stretch more easily, and since NPC has a higher percentage of calcium, it allows for better cell adhesion.

The markers used in this study were selected to characterize osteogenic differentiation; RUNX2 is a transcription factor that is involved in regulating osteoblast differentiation and skeletal

 doi:10.20944/preprints202306.0037.v1

morphogenesis [32]. RUNX2 is known to be an early marker of osteoblast differentiation [33]. RUNX2 mRNA levels are upregulated in the early stages and are downregulated in the terminal stages [34]. OCN, a non-collagenous protein, also regulates hard tissue calcification and calcium ion homeostasis and is considered a final differentiation marker of bone regeneration [32, 34]. RUNX2 mRNA levels were upregulated in the NPC and MTA groups from days 3 to 6. Furthermore, the OCN mRNA level at day 6 was significantly higher in the NPC group than in the control and MTA groups. These results suggest that NPC has a high calcification capacity. Further studies are needed to characterize these effects at other time points. Although there have been many reports on OCN expression in the PDL in response to NPC, there are very few studies on Runx2 expression in the PDL in response to NPC, so we decided to focus on Runx2 in our in vivo experiments in this study. In vivo immunohistochemical studies showed Runx2-positive cells in the PDL adjacent to the perforation. Cells in the PDL have been reported to differentiate into osteoblasts [35]. NPC has a higher amount of calcium content than MTA, and the nanoparticles it contains may have influenced the expression of Runx2 in the PDL in contact with the material because the particles are fine and easily penetrate the perforations in the perforated floor of the pulp chamber. Further, Runx2 is upregulated in the early stages, which is consistent with the results of our in vitro study. In addition, NPC may stimulate the expression of cell differentiation factors, including Runx2, to promote osteoblast differentiation and consequently bone formation.

RANKL was initially identified as a plasma membrane-bound ligand that stimulates osteoclast differentiation and bone resorption. RANKL binds to RANK receptors on the surfaces of monocytes and macrophages, inducing their differentiation into mature multinucleated osteoclasts with bone resorption activity [36, 37]. The action of RANKL can be inhibited by a natural inhibitor, OPG, which is expressed primarily on some epithelial cells, vascular endothelial cells and lymphoid cells [38]. OPG blocks RANKL/RANK interactions, thereby inhibiting osteoclast activation and bone resorption and a decrease in the RANKL/OPG ratio was detected in a previous study [39], which is consistent with the results of this study. The results of TRAP staining, used as an osteoclast marker, also showed a decrease in TRAP-positive cells in the NPC group from days 7 to 28. NPC and MTA have been reported to be involved in the regulation of inflammatory cells and in the promotion of fibroblast and osteoblast differentiation [21]. A decrease in TRAP-positive cells is responsible for decreased bone resorption. These results suggest that MTA and NPC induce osteoblast differentiation and activation and demonstrate osteogenic potential.

In our in vivo experiments, inflammatory cells were observed in the PDL at the cement area in all groups at day 7, but inflammatory cells decreased by day 28. In addition, a line of osteoblasts was observed on the alveolar bone surface in the MTA and NPC groups from day 14, suggesting that MTA and NPC may have promoted osteoblast differentiation. Moreover, an epithelial layer was observed in the control group at days 14 and 28. The perforation of rat molars may stimulate the proliferation of the junctional epithelium [21]. Previous in vivo studies have reported epithelial invasion in MTA and NPC [21]. Nakauchi et al. reported that Malassez's epithelial rest cells normally present in the PDL of the pulp chamber floor may be involved in epithelialization in rats [22]. Considering the results of this study, we believe that the sufficient thickness of the temporary sealing material in this study provided a sufficiently high alkaline environment and prevented the proliferation of epithelial cells in the MTA and NPC groups. In summary, this study lays the groundwork for future investigations of NPC as a perforation repair material in experimental models. Further clinical trials should be performed to better elucidate the effects of NPC in conventional endodontic treatments.

5. Conclusions

In our in vivo experiments, the calcium ion concentration in the medium showed the highest value in the NPC group. Similarly, ARS staining revealed that the NPC group produced significantly more calcified deposits than the MTA group. RUNX2 mRNA levels were upregulated in the NPC and MTA groups from days 3 to 6. Furthermore, the OCN mRNA level at day 6 was significantly higher in the NPC group than in the control and MTA groups. Our in vivo experiments showed that

 doi:10.20944/preprints202306.0037.v1

NPC has a higher calcium content than MTA, and the nanoparticles it contains may have influenced the expression of Runx2 in the PDL in contact with the material because the particles are fine and easily penetrate the perforations in the perforated floor of the pulp chamber. Also, Runx2 is upregulated in the early stages, which is consistent with the results of our in vitro study. These results suggest that NPC may promote the differentiation of periodontal ligament fibroblasts into osteoblasts at an earlier stage than MTA due to the presence of nanoparticles. However, further studies are required to elucidate the specific mechanism of action of NPC in osteogenic differentiation.

Author Contributions: Conceptualization, K.M. and N.E.; methodology, N.E., Y.A., K.N., K.K., M.F., K.M.; investigation, N.E.; writing—original draft preparation, N.E.; writing—review and editing. All authors have read and agreed to the published version of the manuscript.

Funding: This research received no external funding.

Informed Consent Statement: Not applicable.

Data Availability Statement: Not applicable.

Acknowledgments: The authors thank Professors Takashi Muramatsu, Seikou Shintani and Hitoshi Yamamoto, Tokyo Dental College, for their helpful discussions.

Conflicts of Interest: The authors declare no conflicts of interest associated with this manuscript.

References

1. Mente, J.; Leo, M.; Panagidis, D.; Saure, D.; Pfefferle, T. Treatment outcome of mineral trioxide aggregate: repair of root perforations-long-term results. *J. Endod.* **2014**; *40*: 790-796. [https://doi.org/10.1016/j.joen.2014.02.003]
2. Morinaga, K. Histo-pathological studies of periodontal tissue reactions to perforations in the furcation of dogs' teeth treated with various materials and agents. *Shikwa Gakuho* **1989**; *89*: 1107-1116.
3. Shiraiwa, K. Ultrastructural studies of periodontal tissue reaction to Ca $(OH)_2$ preparation and dentin chips for furcation perforations of dogs' teeth. *Jpn. J. Conserv. Dent* **1994**; *37*: 1800-1825.
4. Lee SJ.; Monsef, M.; Torabinejad, M. Sealing ability of a mineral trioxide aggregate for repair of lateral root perforations. *J. Endod.* **1993**; *19*: 541-544. [https://linkinghub.elsevier.com/retrieve/pii/S0099239906812823]
5. Bosso-Martelo, R.; Guerreiro-Tanomaru, JM.; Viapiana, R.; Berbert, FL.; Duarte, MA.; Tanomaru-Filho, M. Physicochemical properties of calcium silicate cements associated with microparticulate and nanoparticulate radiopacifiers. *Clin. Oral Invest.* **2016**; *20*: 83-90. [http://link.springer.com/10.1007/s00784-015-1483-7]
6. Campi, LB.; Rodrigues, EM.; Torres, FFE.; Reis, JMDSN.; Guerreiro-Tanomaru, JM.; Tanomaru-Filho, M. Physicochemical properties, cytotoxicity and bioactivity of a ready-to-use bioceramic repair material. *Braz. Dent. J.* **2023** *34*: 29-38. [https://pubmed.ncbi.nlm.nih.gov/36888842]
7. Maeda, H.; Nakano, T.; Tomokiyo, A.; Fujii, S.; Wada, N.; Monnouchi, S.; Hori, K.; Akamine, A. Mineral trioxide aggregate induces bone morphogenetic protein-2 expression and calcification in human periodontal ligament cells. *J. Endod.* **2010**; *36*: 647-652. [http://dx.doi.org/10.1016/j.joen.2009.12.024]
8. Camiller, J.; Montesin, F. E.; Papaioannou, S.; McDonald, F.; Pitt Ford, T. R. Biocompatibility of two commercial forms of mineral trioxide aggregate. *Int. Endod. J.* **2004**; *37*: 699-704. [https://onlinelibrary.wiley.com/doi/10.1111/j.1365-2591.2004.00859.x]
9. Grazziotin-Soares, R.; Nekoofar, M. H.; Davies, T. E.; Bafail, A.; Alhaddar, E.; Hübler, R.; Busato, A. L.S. Effect of bismuth oxide on white mineral trioxide aggregate: chemical characterization and physical properties. *Int. Endod. J.* **2014**; *47*: 520-533. [https://onlinelibrary.wiley.com/doi/10.1111/iej.12181]
10. Malkondu Ö.; Kazandağ, M. K.; Kazazoğlu, E. A review on biodentine, a contemporary dentine replacement and repair material. *Biomed. Res. Int.* **2014**. [http://www.hindawi.com/journals/bmri/2014/160951/]
11. Jung, Y.; Yoon, J. Y.; Patel, K. D.; Lee, H. H.; Ma, L.; Kim, J.; Lee, J. H.; Shin, J. Biological effects of tricalcium silicate nanoparticle-containing cement on stem cells from human exfoliated deciduous teeth. *Nanomaterials (Basel)* **2020**; *10*: 1373. [https://www.mdpi.com/2079-4991/10/7/1373]
12. Escobar-García, D. M.; Aguirre-López, E.; Méndez-González, V.; Pozos-Guillén, A. Cytotoxicity and initial biocompatibility of endodontic biomaterials (MTA and Biodentine™) used as root-end filling materials. *Biomed. Res. Int.* **2016**; 1-7. [http://www.hindawi.com/journals/bmri/2016/7926961/]

13. Akbulut, MB.; Arpaci, P. U.; Eldeniz, A. U. Effects of four novel root-end filling materials on the viability of periodontal ligament fibroblasts. *Restor. Dent. Endod.* **2018**; *43*: e24. [https://rde.ac/DOIx.php?id=10.5395/rde.2018.43.e24]
14. Rajasekharan, S.; Martens, L. C.; Cauwels, R. G. E. C.; Anthonappa, R. P. Biodentine™ material characteristics and clinical applications: a 3-year literature review and update. *Eur. Arch. Paediatr. Dent.* **2018**; *19*: 1-22. [https://doi.org/10.1007/s40368-018-0328-x]
15. Alqassab, F.; Atmeh, A. R.; Aldossary, N.; Alzahrani, N.; Madi, M.; Omar, O. Inflammatory and differentiation cellular response to calcium silicate cements: An in vitro study. *Int. Endod. J.* **2023**; *56*: 593-607. [https://onlinelibrary.wiley.com/doi/10.1111/iej.13894]
16. Kim, J.M.; Choi, S.; Kwack, K. H.; Kim, S. Y.; Lee, H. W.; Park, K. G protein-coupled calcium-sensing receptor in a crucial mediator of MTA-induced biological activities. *Biomater.* **2017**; *127*: 107-116. [http://dx.doi.org/10.1016/j.biomaterials.2017.02.038]
17. Pedano, M. S.; Li, X.; Li, S.; Sun, Z.; Cokic, S. M.; Putzeys, E.; Yoshihara, K.; Yoshida, Y.; Chen, Z.; Van Landuyt, Ki.; Van Meerbeek, B. Freshly mixed and setting calcium-silicate cements stimulate human dental pulp cells. *Dent. Mater. J.* **2018**; *34*: 797-808. [http://dx.doi.org/10.1016/j.dental.2018.02.005]
18. Manaspon, C.; Jongwannasiri, C.; Chumprasert, S.; Sa-Ard-Iam, N.; Mahanonda, R.; Pavasant, P.; Porntaveetus, T.; Osathanon, T. Human dental pulp stem cell responses to different dental pulp capping materials. *BMC Oral Health* **2021**; *21*: 1-13. [https://doi.org/10.1186/s12903-021-01544-w]
19. Lee, B.N.; Lee, K. N.; Koh, J. T.; Min, K. S.; Chang, H. S.; Hwang, I. N.; Hwang, Y. C.; Oh, W. M. Effects of 3 endodontuc bioactive cements on osteogenic differentiation in mesenchymal stem cells. *J. Endod.* **2014**; *40*: 1217-1222. [http://dx.doi.org/10.1016/j.joen.2014.01.036]
20. Zeid, A.; OS, A.; MK, Y. Biodentine and mineral trioxide aggregate: an analysis of solubility, pH changes and leaching elements. *J. Life Sci. Res.* **2015**; *12*: 18-23.
21. da Fonseca, T. S.; Silva, G. F.; Guerreiro-Tanomaru, J. M.; Delfino, M. M.; Sasso-Cerri, E.; Tanomaru-Filho, M. Biodentine and MTA modulate immunoinflammatory response favoring bone formation in sealing of furcation perforations in rat molars. *Clin. Oral Invest.* **2019**; *23*: 1237-1252. [http://link.springer.com/10.1007/s00784-018-2550-7]
22. Nakauchi, A.; Shintani, S.; Kokubu, E.; Nakajima, K.; Matsuzaka, K.; Inoue, T. Expression of Cytokeratin in Experimentally Created Inflammatory Cyst in Vivo and in Vitro. *Bull. Tokyo Dent. Coll.* **2019**; *60*: 267-277. [https://www.jstage.jst.go.jp/article/tdcpublication/60/4/60_2018-0059/_article]
23. Han, L.; Okiji, T. Uptake of calcium and silicon released from calcium silicate-based endodontic materials into root canal dentine. *Int. Endod. J.* **2011**; *44*: 1081-1087. [https://onlinelibrary.wiley.com/doi/10.1111/j.1365-2591.2011.01924.x]
24. Li, X.; Yoshihara, K.; De Munck, J.; Cokic, S.; Pongprueksa, P.; Putzeys, E.; Pedano, M.; Chen, Z.; Van Landuyt, K.; Van Meerbeek, B. Modified tricalcium silicate cement formulations with added zirconium oxide. *Clin. Oral Invest.* **2017**; *3*: 895-905. [http://link.springer.com/10.1007/s00784-016-1843-y]
25. Ürkmez, E. Ş.; Pınar Erdem, A. Bioactivity evaluation of calcium silicate-based endodontic materials used for apexification. *Aust. Endod. J.* **2020**; *46*: 60-67. [https://onlinelibrary.wiley.com/doi/10.1111/aej.12367]
26. Muramatsu, T.; Kashiwagi, S.; Ishizuka, H.; Matsuura, Y.; Furusawa, M.; Kimura, M.; Shibukawa, Y. Alkaline extracellular conditions promote the proliferation and mineralization of a human cementoblast cell line. *Int. Endod. J.* **2019**; *52*: 639-645. [https://onlinelibrary.wiley.com/doi/10.1111/iej.13044]
27. Giovanna, M. G.; Perut, F.; Ciapetti, G.; Mongiorgi, R.; Prati, C. New Portland cement-based materials for endodontics mixed with articaine solution: a study of cellular response. *J. Endod.* **2008**; *34*: 39-44. [https://linkinghub.elsevier.com/retrieve/pii/S0099239907008369]
28. Chung, M.; Lee, S.; Chen, D.; Kim, U.; Kim, Y.; Kim, S.; Kim, E. Effects of different calcium silicate cements on the inflammatory response and odontogenic differentiation of lipopolysaccharide-stimulated human dental pulp stem cells. *Materials (Basel)* **2019**; *12*: 1259. [http://www.ncbi.nlm.nih.gov/pubmed/30999582] [http://www.pubmedcentral.nih.gov/articlerender.fcgi?artid=PMC6514726]
29. Bortoluzzi, E. A.; Broon, N. J.; Bramante, C. M.; Felippe, W. T.; Tanomaru Filho, M.; Esberard, R. M. The influence of calcium chloride on the setting time, solubility, disintegration, and pH of mineral trioxide aggregate and white Portland cement with a radiopacifier. *J. Endod.* **2009**; *35*: 550-554. [https://linkinghub.elsevier.com/retrieve/pii/S0099239909000090]
30. Al-Sa'eed, O. R.; Al-Hiyasat, A. S.; Darmani, H. The effects of six root-end filling materials and their leachable components on cell viability. *J. Endod.* **2008**; *34*: 1410-1414. [http://dx.doi.org/10.1016/j.joen.2008.08.001]

31. Akbulut, M. B.; Uyar Arpaci, P.; Unverdi Eldeniz, A. 'Effects of novel root repair materials on attachment and morphological behaviour of periodontal ligament fibroblasts: Scanning electron microscopy observation'. *Microsc. Res. Tech.* **2016**; *79*: 1214-1221. [https://onlinelibrary.wiley.com/doi/10.1002/jemt.22780]
32. Theodoro, L. H.; Caiado, R. C.; Longo, M.; Novaes, V. C. N.; Zanini, N. A.; Ervolino, E.; de Almeida, J. M. Effectiveness of the diode laser in the treatment of ligature-induced periodontitis in rats: a histopathological, histometric, and immunohistochemical study. *Lasers Med. Sci.* **2015**; *30*: 1209-1218. [http://link.springer.com/10.1007/s10103-014-1575-7]
33. Camilleri, S.; McDonald, F. Runx2 and dental development. *Eur. J. Oral Sci.* **2006**; *114*: 361-373. [https://onlinelibrary.wiley.com/doi/10.1111/j.1600-0722.2006.00399.x]
34. Rathinam, E.; Rajasekharan, S.; Chitturi, R. T.; Martens, L.; De Coster, P. Gene expression profiling and molecular signaling of dental pulp cells in response to tricalcium silicate cements: A Systematic Review. *J. Endod.* **2015**; *41*: 1805-1817. [http://dx.doi.org/10.1016/j.joen.2015.07.015]
35. Hiraga, T.; Ninomiya, T.; Hosoya, A.; Takahashi, M.; Nakamura, H. Formation of bone-like mineralized matrix by periodontal ligament cells in vivo: a morphological study in rats. *J. Bone Miner. Metab.* **2009**; *27*: 149-157. [http://link.springer.com/10.1007/s00774-009-0039-9]
36. Takayanagi H. New developments in osteoimmunology. *Nat. Rev. Rheumatol.* **2012**; *8*: 684-689.
37. Petean, I. B. F.; Küchler, E. C.; Soares, I. M. V.; Segato, R. A. B.; Silva, L. A. B.; Lívia, A. A. Genetic polymorphisms in RANK and RANKL are associated with persistent apical periodontitis. *J. Endod.* **2019**; *45*: 526-531. [https://linkinghub.elsevier.com/retrieve/pii/S009923991930038X]
38. Terpos, E.; Ntanasis-Stathopoulos, I.; Gavriatopoulou, M.; Dimopoulos, M. A. Pathogenesis of bone disease in multiple myeloma: from bench to bedside. *Blood Cancer J.* **2018**; *8*: 7. [http://dx.doi.org/10.1038/s41408-017-0037-4]
39. Eraković, M.; Duka, M.; Bekić, M.; Tomić, S.; Ismaili, B.; Vučević, D.; Čolić, M. Anti-inflammatory and immunomodulatory effects of Biodentine on human periapical lesion cells in culture. *Int. Endod. J.* **2020**; 53: 1398-412. [https://onlinelibrary.wiley.com/doi/10.1111/iej.13351]